

Proposal for a realtime Einstein-synchronization-defined satellite virtual clock

Chenhao Yan(严晨皓), Xueyi Tang(汤雪逸), Shiguang Wang(王时光), Lijiaoyue Meng(孟李皎悦), Haiyuan Sun(孙海媛), Yibin He(何奕彬), and Lijun Wang(王力军)

Citation: Chin. Phys. B, 2024, 33 (**7**): 070601. DOI: 10.1088/1674-1056/ad3dc9
Journal homepage: http://cpb.iphy.ac.cn; http://iopscience.iop.org/cpb

What follows is a list of articles you may be interested in

A redundant subspace weighting procedure for clock ensemble

Hai Xu(徐海), Yu Chen(陈煜), Mo-Chi Liu(刘默驰), and Yu-Zhuo Wang(王玉琢)
Chin. Phys. B, 2024, 33 (**4**): 040601. DOI: 10.1088/1674-1056/ad1b43

Robust free-space optical frequency transfer in time-varying link distances conditions

Zhou Tong(童周), Lei Liu(刘雷), Jia-Liang Wang(王家亮), Qian Cao(操前), Zhi-Cheng Jin(金志成), Kang Ying(应康), Shen-Sheng Han(韩申生), Zheng-Fu Han(韩正甫), and You-Zhen Gui(桂有珍)
Chin. Phys. B, 2024, 33 (**2**): 020601. DOI: 10.1088/1674-1056/ad0718

Sympathetic electromagnetically induced transparency ground state cooling of a $^{40}Ca^{+}$–$^{27}Al^{+}$ pair in an $^{27}Al^{+}$ clock

Chenglong Sun(孙成龙), Kaifeng Cui(崔凯枫), Sijia Chao(晁思嘉), Yuanfei Wei(魏远飞), Jinbo Yuan(袁金波), Jian Cao(曹健), Hualin Shu(舒华林), and Xueren Huang(黄学人)
Chin. Phys. B, 2023, 32 (**5**): 050601. DOI: 10.1088/1674-1056/aca39d

Measurements of Majorana transition frequency shift in caesium atomic fountain clocks

Jun-Ru Shi(施俊如), Xin-Liang Wang(王心亮), Fan Yang(杨帆), Yang Bai(白杨), Yong Guan(管勇), Si-Chen Fan(范思晨), Dan-Dan Liu(刘丹丹), Jun Ruan(阮军), and Shou-Gang Zhang(张首刚)
Chin. Phys. B, 2023, 32 (**4**): 040602. DOI: 10.1088/1674-1056/ac8344

Precise measurement of ^{171}Yb magnetic constants for $^{1}S_0$–$^{3}P_0$ clock transition

Ang Zhang(张昂), Congcong Tian(田聪聪), Qiang Zhu(朱强), Bing Wang(王兵), Dezhi Xiong(熊德智), Zhuanxian Xiong(熊转贤), Lingxiang He(贺凌翔), and Baolong Lyu(吕宝龙)
Chin. Phys. B, 2023, 32 (**2**): 020601. DOI: 10.1088/1674-1056/aca14e

---

Proposal for a realtime Einstein-synchronization-defined satellite virtual clock

Chenhao Yan(严晨皓)[1], Xueyi Tang(汤雪逸)[1], Shiguang Wang(王时光)[1,†], Lijiaoyue Meng(孟李皎悦)[1], Haiyuan Sun(孙海媛)[1], Yibin He(何奕彬)[1], and Lijun Wang(王力军)[1,2,‡]

[1] *Department of Precision Instrument, Tsinghua University, Beijing* 100091, *China*
[2] *Department of Physics, Tsinghua University, Beijing* 100091, *China*

(Received 7 January 2024; revised manuscript received 18 March 2024; accepted manuscript online 12 April 2024)

Realization of high performance satellite onboard clock is vital for various positioning, navigation, and timing applications. For further improvement of the synchronization-based satellite time and frequency references, we propose a geosynchronous (GEO) satellite virtual clock concept based on ground–satellite synchronization and present a beacon transponder structure for its implementation (scheduled for launch in 2025), which does not require atomic clocks to be mounted on the satellite. Its high performance relies only on minor modifications to the existing transponder structure of GEO satellites. We carefully model the carrier phase link and analyze the factors causing link asymmetry within the special relativity. Considering that performance of such synchronization-based satellite clocks is primarily limited by the link's random phase noise, which cannot be adequately modeled, we design a closed-loop experiment based on commercial GEO satellites for pre-evaluation. This experiment aims at extracting the zero-means random part of the ground-satellite Ku-band carrier phase via a feedback loop. Ultimately, we obtain a 1σ value of 0.633 ps (two-way link), following the Gaussian distribution. From this result, we conclude that the proposed real-time Einstein-synchronization-defined satellite virtual clock can achieve picosecond-level replication of onboard time and frequency.

Keywords: Einstein synchronization, satellite virtual clock, geosynchronous satellite, carrier phase

PACS: 06.30.Ft, 84.40.Ua **DOI:** 10.1088/1674-1056/ad3dc9

1. Introduction

Artificial satellite technology is becoming increasingly important in daily life, production, and scientific research.[1–6] Its primary functions encompass communication, positioning, navigation, and timing. In design processes of common communication and navigation satellite payloads, it is essential to equip satellites with a series of high-precision frequency or time references onboard, particularly in scenarios involving high-precision navigation and physics research.[7–14] This is due to the fact that the time or frequency output of the satellite's onboard clock not only provides a reference for the time dissemination of the satellite ephemeris but also supports the operation of a series of onboard radio-frequency (RF) devices and digital systems. With the continuous development of miniaturization technology for atomic clocks, an increasing number of communication and navigation satellites start to incorporate atomic clocks as part of their payloads, which has significantly enhanced the performance of positioning, navigation, and timing (PNT) applications in recent years.[15–19] In addition to the proposal of incorporating atomic clocks into the satellites, for some satellites that are visible to the ground station for a long period of time, stability and high-precision clock references onboard can also be achieved via ground–satellite time and frequency transfer. By establishing an RF link between Earth and the satellite, it is possible to replicate a high-precision reference that is synchronized with the ground time and frequency onboard the satellite. Several efforts have been made based on GNSS constellations, such as Japan's QZSS[20–22] and China's CAPS.[23–25] Synchronization performance on the order of nanoseconds or even subnanoseconds has been achieved.

However, both the aforementioned approaches face technical challenges in further performance improvement. On the one hand, for satellite atomic clocks, although miniaturized atomic clocks can achieve smaller size and mass at the same level of accuracy compared with the past, owing to cost limitations and payload capacity constraints, the demand for enhancing the performance of onboard atomic clocks has been in conflict with the need for size reduction.[12,26] Thus, the volume and mass of some representative state-of-the-art atomic frequency standards are still too large for the current satellite payload capacity, making it difficult to popularize picosecond-level onboard atomic clocks in the near future.[26–30] On the other hand, the existing methods for synchronization-based satellite clock implementation generally can only achieve subnanosecond performance.[20–25] This limitation arises from insufficient analysis and processing of the relativistic effect and onboard crystal oscillator phase variation.

To enhance the precision and availability of

†Corresponding author. E-mail: wangsg@tsinghua.edu.cn
‡Corresponding author. E-mail: lwan@tsinghua.edu.cn

© 2024 Chinese Physical Society and IOP Publishing Ltd

synchronization-based onboard time and frequency references, it is necessary to comprehensively consider factors such as the asymmetry in the two-way link between Earth and the satellite due to relativistic effects and the initial phase or additional phase noise of the transponder's local oscillator. Additionally, the carrier phase technique[31–36] should be incorporated into the payload architecture to improve the synchronization performance.

For improving the performance of time and frequency reference on GEO satellites, this paper proposes the concept of an onboard virtual clock based on satellite Einstein synchronization and the corresponding beacon transponder implementation, which was scheduled for payload launch in 2025. This onboard virtual clock architecture is based on two-way information exchange between Earth and the satellite and does not require the satellite to carry atomic clocks. Only minor modifications to the existing commonly used GEO satellite transparent transponder structure are needed to achieve our proposal. We carefully consider the asymmetry of the two-way rounded link caused by the effects of the special theory of relativity (satellite Einstein synchronization), introduce an unmodulated carrier phase as the information transmission medium, and employ a beacon transponder for the elimination of the onboard oscillator phase variation. Because the unmodeled phase noise level of the Earth–satellite link is the main factor limiting the final precision of the proposed onboard virtual clock architecture in this study, a closed-loop locking experimental system is used to evaluate the phase noise of the commercial Ku-band GEO satellite's Earth–satellite link as a reference, resulting in a Gaussian distribution of 0.633 ps at 1σ. According to comparisons and extrapolations, we believe that the proposed implementation of the onboard virtual clock architecture can achieve frequency synchronization at the picosecond level, which may be useful for high-precision PNT applications and physical experiments.

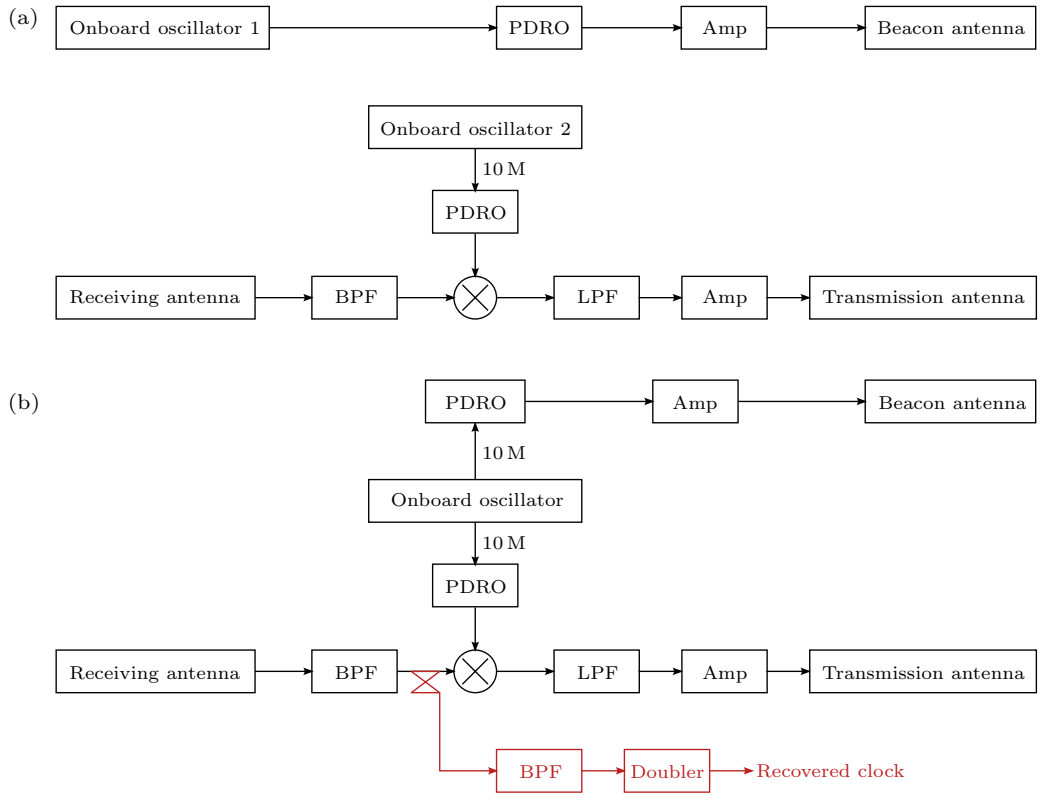


Fig. 1. Comparison of the traditional transponder and the novel transponder with an onboard clock beacon. PDRO: phase-locked dielectric resonator oscillator; Amp: amplifier; BPF: bandpass filter; LPF: lowpass filter; Doubler: phase-locked frequency doubler oscillator circuit.

2. Carrier phase based beacon transponder

Figure 1(b) shows the structure of the beacon transponder, which is used to implement the onboard virtual clock discussed in this study, in comparison with the commonly used communication satellite transponders [Fig. 1(a)]. Although conventional communication satellite transponders also possess beacon transmission functionality, this feature is typically employed by users as a satellite directive beacon for antenna direction adjustment. Because of the modular requirements in the manufacturing of satellite payloads, the beacon reference for such transponders is generally provided by an independently operated onboard crystal oscillator. Thus, the information carried by such beacon beams upon reaching the ground fails to provide the essential phase reference of the satellite

transponder's down-conversion local oscillator. In contrast, the proposed beacon transponder utilizes the one-way channel of the satellite beacon to reduce the influence of the GEO satellite onboard crystal oscillator on the ground–satellite two-way link, by synchronizing the beacon channel's oscillator with the downconversion stage oscillator of the satellite transponder. Consequently, the initial phase of the frequency local oscillator can be determined by extracting the phase information carried by the beacon's down-link carrier beam. This approach effectively resolves the issue of phase drift in the onboard crystal oscillator that arises when the carrier phase is employed as the medium for information transmission.

A schematic depicting the principle of achieving high-precision frequency recovery with the GEO satellite utilizing the beacon transponder is presented in Fig. 2.

To replicate the high-precision time or frequency reference from the ground station to the satellite, a carrier phase bidirectional link called the detection channel, a unidirectional downlink (beacon channel), and an uplink synchronization link (synchronization channel) are employed. For the detection channel, taking the self-receiving and self-transmitting channel of a specific ground station A as an example, considering factors such as the changing relative position between the satellite and the ground, the initial phase of the onboard crystal oscillator, ionospheric effects, and the effects of the theory of relativity, the carrier-phase signal generated by the high-precision time and frequency reference of the ground station is forwarded by the synchronized orbit satellite and subsequently received on the ground. The carrier phase value $\phi_{\mathrm{RX-AA}}$ obtained by the receiver satisfies

$$\begin{aligned}\phi_{\mathrm{RX-AA}} = \phi_{\mathrm{A}}(t) - \omega_{\mathrm{s}}\tau_{\mathrm{s}} - \frac{\omega_{\mathrm{uA}}+\omega_{\mathrm{dA}}}{c}\rho_{\mathrm{as}}(t) + K_{\mathrm{iono}} \\ \times \mathrm{TEC_A}\left(\frac{1}{\omega_{\mathrm{uA}}}+\frac{1}{\omega_{\mathrm{dA}}}\right) + \omega_{\mathrm{s}}\gamma_{\mathrm{A}}\Sigma_{\mathrm{A}},\end{aligned} \tag{1}$$

where $\phi_{\mathrm{A}}(t)$ represents the slow phase drift of the ground station's atomic frequency standard; ω_{s} represents the angular frequency of the satellite transponder's down-link local oscillator; τ_{s} represents the satellite onboard oscillator's phase variation; ω_{uA} and ω_{dA} represent the angular frequencies of satellite up-link and down-link carriers, respectively, with respect to station A; and $\rho_{\mathrm{as}}(t)$ represents the pseudo-distance from station A to the satellite. For the asymmetry of the satellite two-way link in the special theory of relativity, γ_{A} is the correction coefficient for station A's proper time, while Σ_{A} represents the link asymmetry in Minkowski spacetime, which is extensively discussed in the next section. Regarding the ionospheric nonlinear delay factors, $\mathrm{TEC_A}$ represents the total electron content along station A's transmission path, and K_{iono} is the rounded coefficient constant of ionospheric delay, which is given as

$$K_{\mathrm{iono}} = 40.28 \times 4\pi^2/c. \tag{2}$$

By conducting a similar analysis, for the beacon channel in Fig. 2, the carrier phase received on the ground for the down-link carrier beam can be expressed as

$$\phi_{\mathrm{S-A}}(t) = \omega_{\mathrm{ds}}\tau_{\mathrm{s}} - \frac{\omega_{\mathrm{ds}}}{c}\rho_{\mathrm{as}}(t) + \frac{K_{\mathrm{iono}}\cdot\mathrm{TEC_A}}{\omega_{\mathrm{ds}}} - \omega_{\mathrm{ds}}\gamma_{\mathrm{A}}\Sigma_{\mathrm{A}}, \tag{3}$$

where ω_{ds} represents the down-link beacon angular frequency. For Eqs. (1) and (3), it is reasonable to construct a compensatory equation that eliminates the phase drift of the onboard crystal oscillator and offsets the carrier phase value of the synchronization channel in Fig. 2 by employing a linear combination satisfying

$$\begin{aligned}\phi_{\mathrm{ps}}(t) &= -\frac{1}{2}\left[\phi_{\mathrm{S-A}}(t)\cdot\frac{\omega_{\mathrm{s}}}{\omega_{\mathrm{ds}}} + \phi_{\mathrm{RX-AA}}(t)\right] \\ &\quad - \omega_{\mathrm{uA}}\gamma_{\mathrm{A}}\Sigma_{\mathrm{A}} + \frac{K_{\mathrm{iono}}\mathrm{TEC_A}}{\omega_{\mathrm{p1}}} \\ &= \frac{\rho_{\mathrm{as}}(t)\omega_{\mathrm{uA}}}{c} - \frac{K_{\mathrm{iono}}\mathrm{TEC_A}}{\omega_{\mathrm{uA}}} - \frac{1}{2}\phi_{\mathrm{A}}(t) - \omega_{\mathrm{uA}}\gamma_{\mathrm{A}}\Sigma_{\mathrm{A}},\end{aligned} \tag{4}$$

where

$$\omega_{\mathrm{p1}} = \frac{2\omega_{\mathrm{dA}}\omega_{\mathrm{ds}}^2\omega_{\mathrm{uA}}}{\omega_{\mathrm{s}}(\omega_{\mathrm{dA}}^2+\omega_{\mathrm{ds}}^2+\omega_{\mathrm{dA}}\omega_{\mathrm{ds}})}. \tag{5}$$

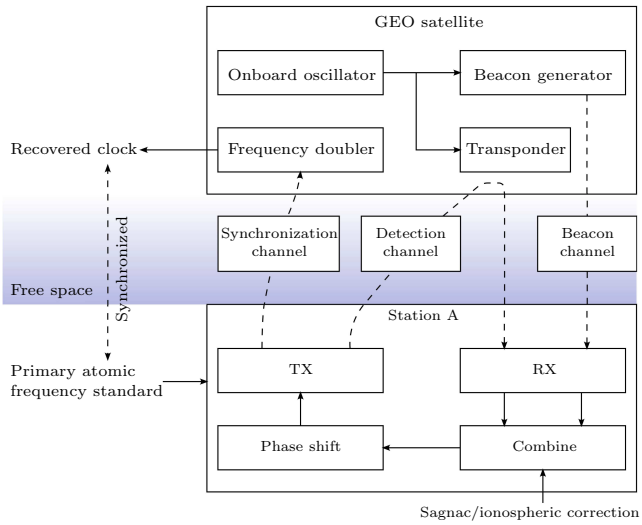


Fig. 2. Schematic of the carrier phase-based beacon transponder's time and frequency recovery.

For the ground station, this equation is sent to an RF phase shifter on the transmitting side of the synchronization channel, which phase shifts the carrier phase at the ground station's transmitter. Consequently, assuming that no significant changes occur in the ground–satellite link in the short term, the synchronization channel's carrier phase received by the GEO satellite can be expressed as

$$\begin{aligned}\phi_{\mathrm{RX}}^{(\mathrm{sc})}(t) = \phi_{\mathrm{ps}}(t) + \phi_{\mathrm{A}}(t) - \frac{\omega_{\mathrm{uA}}}{c}\rho_{\mathrm{as}}(t) + \frac{K_{\mathrm{iono}}\mathrm{TEC_A}}{\omega_{\mathrm{uA}}} \\ + \omega_{\mathrm{uA}}t + \omega_{\mathrm{uA}}\gamma_{\mathrm{A}}\Sigma_{\mathrm{A}}\end{aligned}$$

$$= \frac{1}{2}\phi_{\rm A}(t) + \omega_{\rm uA}t. \tag{6}$$

At this point, the signal received by the satellite can be obtained through an RF coupler, and frequency multiplication is performed to restore and track the phase variations of the high-precision frequency reference at the ground station in real time. As the system operates in a stable state, phase fluctuations in the ground station's atomic clock can be synchronized with the satellite owing to the real-time phase-shift operation of the synchronization channel in Fig. 2. Consequently, the frequency standard at the ground station can be recovered at the satellite's receiving side, providing both the initial phase and the phase-fluctuation information for further use.

3. Asymmetry of satellite two-way link in special theory of relativity

For synchronization-based satellite time and frequency references, if nanosecond-level performance is required, it will be unnecessary to correct for the special theory of relativity. However, if further improvements in precision and accuracy are desired, careful analysis and handling of the asymmetric factors in the uplink and downlink due to relativistic effects will be needed, with real-time corrections applied. The beacon transponder described in the above section utilizes two-way information exchange between the ground and the satellite. The timing values of each point in the recovered clock are determined by the round-trip time of the signal between the ground station and the satellite. This determination method is commonly known as Einstein synchronization in the inertial reference frame. The reference source of the satellite clock (such as an atomic clock providing transition frequencies at the ground station) does not actually exist on the satellite; rather, it conceptualizes a virtual clock defined in real time by the Einstein synchronization. However, because classical Einstein synchronization is not applicable in non-inertial reference frames, some corrections mentioned in this section must be incorporated. This involves reanalyzing the process of two-way information exchange between the ground and the satellite in the framework of special relativity to determine the values of $\gamma_{\rm A}$ and $\Sigma_{\rm A}$ in Eq. (4).

Figure 3 shows a single two-way information-exchange process in Minkowski spacetime. Because both Earth and the GEO satellites in Earth-centered inertial (ECI) frames make rotational motion approximately along the north–south polar line, one dimension of Earth is dropped, and the time axis is employed as a substitute, resulting in a three-dimensional geometric problem, for better presentation. The equidistant helix G is the world line (in Einstein's special theory of relativity) of the ground station, while the points G_1, G_2, G_3, and G_4 represent the ground station's statuses at the coordinate time of signal emission (τ_1), the coordinate time of signal arrival at the GEO satellite (τ_2), the coordinate time of signal transmission from the GEO satellite (τ_3), and the coordinate time of signal reception (τ_4) in the ECI reference system.

Owing to the high-speed motion of both the GEO satellite and the ground station in the ECI reference frame, the geometric structures of the paths traveled by the information during the uplink and down-link processes differ, resulting in different transmission delays. By expressing this asymmetry in terms of the coordinate time in the ECI frame, the following results can be obtained through geometric analysis:

$$\Sigma_{\rm A} = \frac{1}{2}[(\tau_4 - \tau_2) - (\tau_2 - \tau_1)] = -\frac{r_{\rm e} r_{\rm s} \omega_0 \sin\theta_0}{c^2 - r_{\rm e} r_{\rm s} \omega_0^2 \cos\theta_0}, \tag{7}$$

where ω_0 represents the rotational angular velocity of Earth; $r_{\rm e}$ and $r_{\rm s}$ represent the distances from the projection point of the ground station and the satellite, respectively, on the equatorial plane to the center of Earth; θ_0 represents the difference in longitude between the ground station and the satellite; and c represents the speed of light in vacuum.

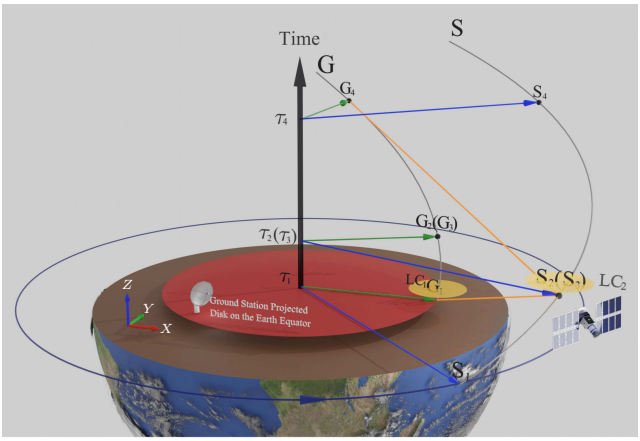


Fig. 3. Demonstration of the asymmetry of a single two-way information exchange between a ground station and a satellite.

As the ground–satellite link is established with high-precision atomic frequency standards located on Earth's surface as the reference, the asymmetric delays expressed by Eq. (7) in terms of coordinate time are actually perceived by the ground station in its proper time. Thus, when performing measurements and corrections at the ground-station terminals, adjustments related to the time dilation factor associated with the position coordinates of the ground station in special relativity must be performed, satisfying

$$\gamma_{\rm A} = \frac{\sqrt{c^2 - \omega_0^2 r_{\rm e}^2}}{c}. \tag{8}$$

The above two equations constitute corrections to the classical Einstein synchronization in the two-way information-exchange process between the ground and the GEO satellite, which are defined in the following.

Satellite Einstein synchronization In the realm of ECI, consider the process of two-way signal transmission between

a GEO satellite and ground station A, which entails three distinct events: the signal's emission from the ground station, its traversal through the channel to reach the satellite, and its subsequent return to the ground station. These events are measured locally at the ground station and denoted as $T_1^{(g)}$, $T_2^{(g)}$, and $T_4^{(g)}$, respectively. In the occasion that for every occurrence of two-way signal transmission via the satellite, a certain satellite time reference $\hat{T}_s$ aligns constantly with $T_2^{(g)}$, it can be concluded that in the ECI reference frame, this time reference remains synchronized with the standard clock reference at the ground station. Consequently, the following equations hold true for $\hat{T}_s$:

$$\begin{aligned}\hat{T}_s &= \frac{1}{2}(T_1^{(g)} + T_4^{(g)}) - \Sigma_A \cdot \gamma_A,\\ \Sigma_A &= -\frac{r_e r_s \omega_0 \sin\theta_0}{c^2 - r_e r_s \omega_0^2 \cos\theta_0},\\ \gamma_A &= \frac{\sqrt{c^2 - \omega_0^2 r_e^2}}{c}.\end{aligned} \tag{9}$$

The basic idea of Eq. (9) is to use the occurrence of the signal reaching the satellite as a synchronization timestamp between the ground station and the satellite. For this event, the proper time of the ground station should be measured as $T_2^{(g)}$, while the satellite receiver, upon detecting the arrival of the signal at the satellite, defines its own time as $\hat{T}_s$, which happens to be equal to $T_2^{(g)}$. Furthermore, in practical situations, it is impossible for the ground station to perceive the event of the signal reaching the satellite in real time. Therefore, the significance of Eq. (9) lies in the fact that the definition of time on the satellite relies solely on the data that the ground station can acquire (i.e., the transmission time of the signal and the time it is received by the ground station) and the precise ephemeris of the satellite, rather than real-time measurements of the event of the signal reaching the satellite.

4. Random phase noise evaluation on commercial Ku-band two-way satellite links

Owing to the continuous reliance of synchronization-based satellite time and frequency references on ground–satellite communication, the performance of the satellite virtual clock depends significantly on the carrier beam quality and phase noise level of the RF link. Most of the interference in the link channels arises from random perturbations in the space medium, which are often difficult to model accurately. Therefore, we conducted experiments to evaluate the random phase noise in the carrier phase link of Earth GEO orbits and commercial GEO satellites. This was conducted as a pre-validation before the launching of the beacon transponder payload, to assess the performance that can potentially be achieved with the existing software-defined radio equipment.

The core concept of our closed-loop carrier phase experiment and its difference from the original clock recovery system are shown in Fig. 4. Figure 4(a) presents the scheme of our original clock recovery link. The signal-transmission process comprises two uplink steps and two down-link steps. Figure 4(b) shows the closed-loop experiment aimed at evaluating the total random noise along the ground–satellite link, which contains one uplink step and a down-link step. Because of the zero-mean nature of random noise, it is mostly averaged by the integrator, leaving only the non-random components (such as satellite motion, effects of special relativity, and ionospheric delay) at the input of the controller. Thus, the behavior of the feedback loop gradually tends to cancel out the non-random phase variations of the entire ground–satellite link through the pre-transmission phase shifting stage on the TX side. Ultimately, when the entire closed-loop link reaches a steady state, the random phase jitter of a two-way carrier phase link is accumulated at the receiving end of the ground station's closed-loop link. On this basis, the recover noise at the satellite in Fig. 4(a) can be regarded as $\sqrt{2}$ times the acquired result σ_r in Fig. 4(b).

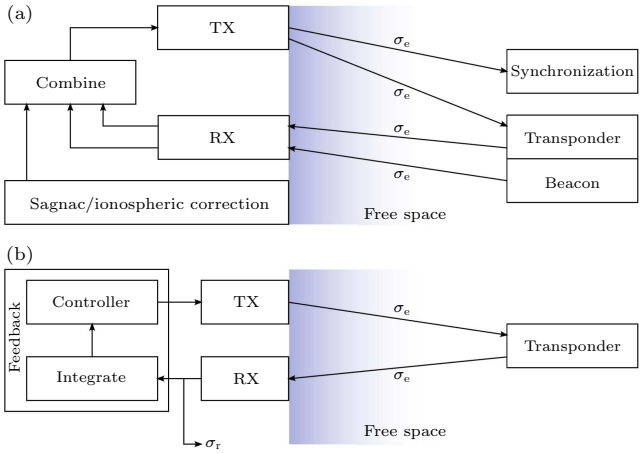


Fig. 4. Comparison of the proposed frequency recovery system and the phase noise evaluation experiment: (a) link noise in our proposed system based on carrier phase beacons in actual operation, where σ_e represents the one-way random noise error; (b) link noise of the closed-loop bidirectional carrier phase locking experiment performed in this study.

For the specific hardware implementation, figure 5 presents the hardware diagram of the Ku-band transceiver and the baseband processing device. We take the China Sat 10 as the test satellite, with an uplink frequency of 14.3135 GHz and a down-link frequency of 12.5635 GHz. The height of the satellite orbit is approximately 35800 km, which is roughly the same as that of the satellite to be carrying the aforementioned beacon transponder. The frequency up-conversion system we utilize contains a vector signal generator (VSG) for L-band generation and a block upconverter for L band-to-Ku band amplification. The frequency down-conversion system uses a three-step demodulation structure to acquire the baseband signal. All the RF wave generation devices in Fig. 5 are

referenced to an active hydrogen maser, which acts as the primary frequency standard in our experiment.

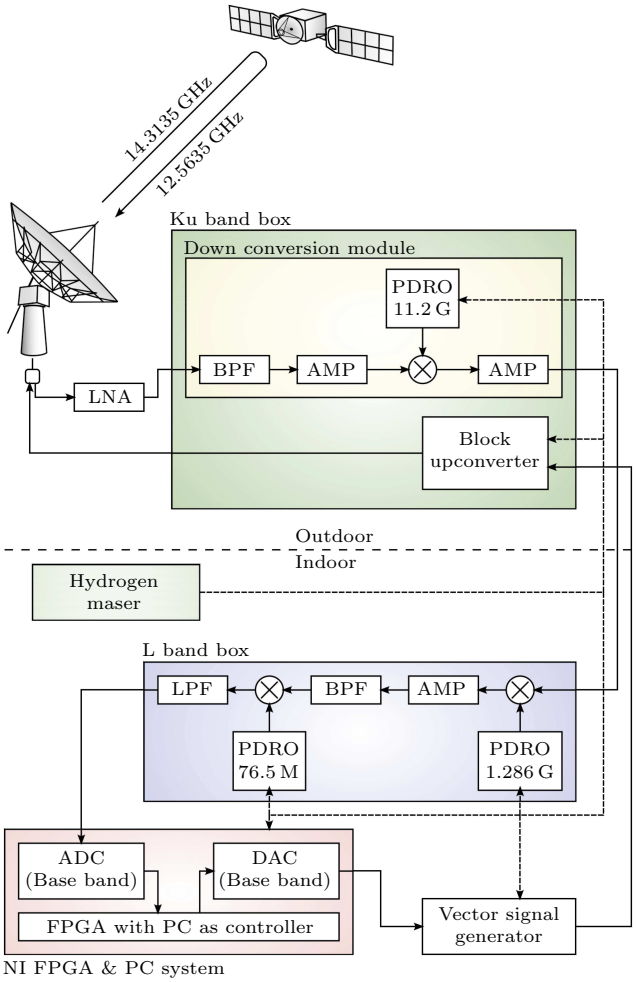


Fig. 5. Schematic of the Ku-band transceiver and the signal-processing device. PDRO: phase-locked dielectric resonator oscillator; AMP: amplifier; BPF: bandpass filter; LPF: low-pass filter; LNA: low-noise amplifier; ADC: analog-to-digital converter; DAC: digital-to-analog converter; FPGA: field-programmable gate arrays; PC: personal computer.

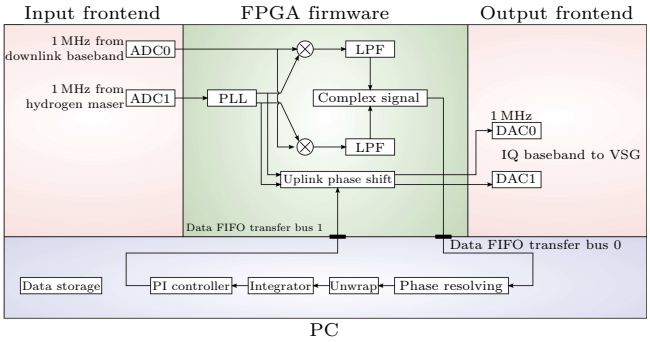


Fig. 6. FPGA firmware. ADC: analog-to-digital converter; DAC: digital-to-analog converter; LPF: lowpass filter; PLL: phase-locked loop.

Figure 6 presents the baseband signal processing system realized using NI field-programmable gate array (FPGA) hardware. We use a digital IQ demodulator and an uplink baseband generator in the FPGA board, whose global clock is also referenced to the external root hydrogen maser. Furthermore, we use a data first-in-first-out (FIFO) pipeline for communication between the FPGA and PC devices. This pipeline can significantly reduce the instability caused by the thread preemption on the PC's operating system. In the PC compensation program shown in Fig. 6, the phase of the down-link signal is first extracted from the IQ complex signal. Subsequently, the extracted phase is sent to a phase unwrapper followed by an integrator and a proportional-integral controller. We introduce these steps on the PC to satisfy the requirements of floating-point value processing, flow control, and data storage. NI LabVIEW is used for the programming of the PC software and the configuration of the FPGA.

5. Results

Figure 7 shows the time-domain waveform for the residual phase of our closed-loop compensation experiment, which was acquired as σ_r in Fig. 4(b). This experiment started on Nov 10, 2022 at 03:34:51 UTC and lasted approximately 7 d. We performed a statistical analysis on the phase values obtained in this time-domain result and grouped all the data into 128 bins, as shown in Fig. 8(a). From Fig. 8(a), we assume that the two-way noise of the ground–satellite link conforms to a probabilistic model with a Gaussian distribution, and Fig. 8(b) shows the corresponding Gaussian fit curve. The fitting result is calculated by

$$P(\phi) = \exp\Big[-\frac{1}{2}\Big(\frac{\phi - 0.000081}{0.05}\Big)^2\Big], \tag{10}$$

where ϕ represents the down-link residual phase in rad, and $P(\phi)$ represents the probability statistics value of the down-link phase ϕ under closed-loop conditions.

For verifying our assumption, the Shapiro–Wilk test was used to evaluate the normality of the ground–satellite link phase residual. The W statistic is calculated by

$$W = \frac{(\sum_{i=1}^{n} a_i x_{(i)})^2}{\sum_{i=1}^{n}(x_i - \bar{x})^2}, \tag{11}$$

where $x_{(i)}$ represents the ascending ordered phase value shown in Fig. 7, and a_i represents the rounded factor obtained from the fitted normal distribution.[37] A W statistic of 0.99974 with a p value of 0.82266 is obtained, which indicates considerable conformity between the satellite ground link phase noise and the corresponding normal distribution.

From Eq. (10), the σ value is determined to be 0.05 rad, which indicates a time fluctuation of 0.633 ps at a down-link Ku-band frequency of 12.5635 GHz. This result indicates that for a two-way electromagnetic-wave transmission process, link noise of < 1 ps can be achieved. Thus, a frequency reproduction precision of 0.896 ps is promising in our frequency reproduction scheme, which contains a four-way transmission model, as shown in Fig. 4.

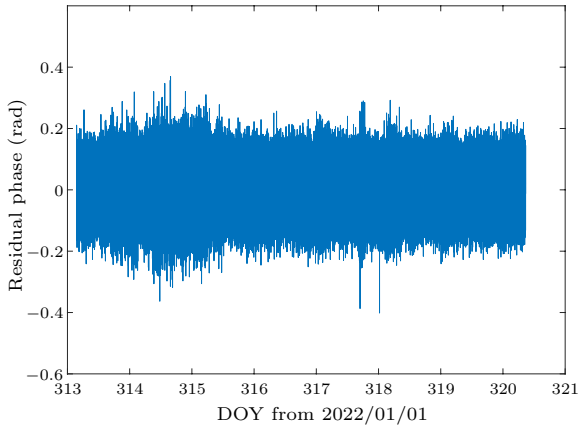


Fig. 7. Ku-band phase residuals of the closed-loop experiment.

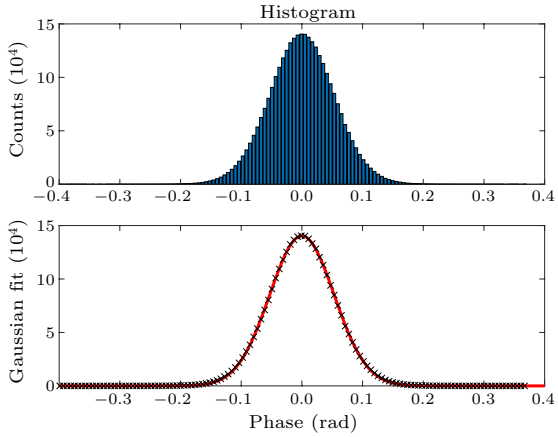


Fig. 8. Histogram and Gaussian fitting of the statistical results.

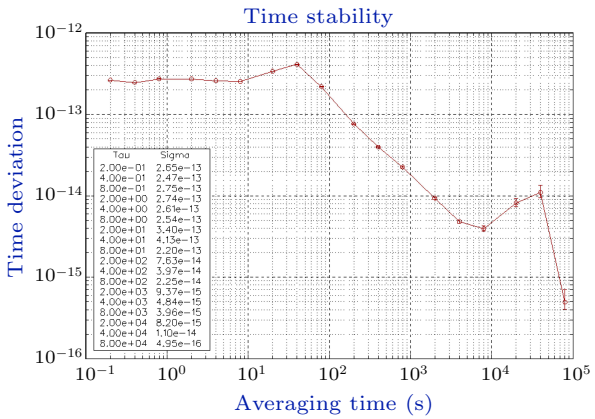


Fig. 9. Time deviation of the closed-loop experiment in the Ku band.

Figure 9 shows the time deviation of the residual phase. Two bulges were observed over the 7-d experiment. We attribute the bulge at approximately 3×10^4 s to the periodic motion of the satellite and the cyclic changes in the outdoor temperature. We have no reasonable explanation for the bulge at approximately 30 s, but we suspect that it could be correlated with the time constant of our feedback loop owing to the alignment with the integral time of the proportional-integral-derivative module employed in the system feedback loop, which has a similar duration scale ($P = 0.01$, $T_\mathrm{i} = 0.3$ min, and $T_\mathrm{d} = 0.3$ min).

Figure 10 shows the Allan deviation for the residual phase. Notably, the slope of $1/\tau$ decreases with an increase in the average time. The second-level stability reaches approximately 10^{-12}, while the day-level stability approaches 10^{-16}.

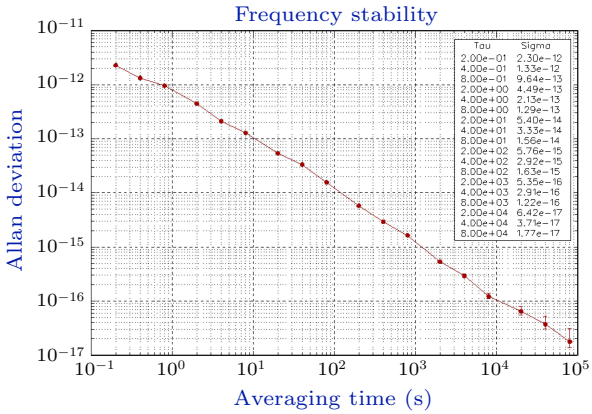


Fig. 10. Allan deviation of the closed-loop experiment in the Ku band.

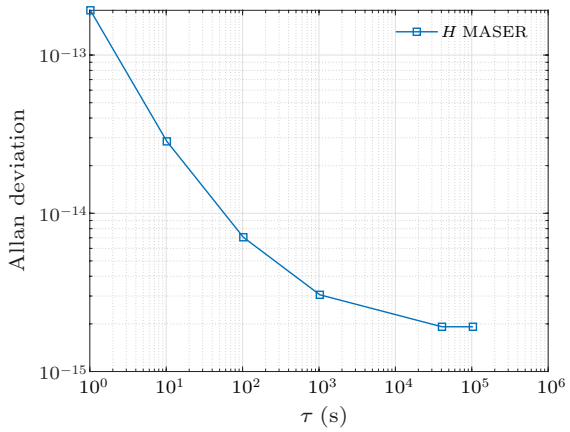


Fig. 11. Allan deviation of the hydrogen maser used in the experiment.

Figure 11 shows the Allan deviation of the active hydrogen maser used in the closed-loop experiment. For a closed-loop carrier phase system shown in Fig. 5, carrier phase comparison of the transmitting and receiving ends is needed to obtain the phase result. During the signal transmission period, the stability of the hydrogen maser is required to ensure the correctness of the carrier phase measurement. Comparing Figs. 11 and 10 reveals that the short-time stability of the hydrogen maser is at least one order of magnitude higher than the closed-loop experimental results. Thus, the frequency reference did not affect the final measurement.

6. Discussion

The results obtained in the closed-loop experiment indicate that the current ground–satellite carrier link can support synchronization-based satellite time and frequency reference with ps-level precision, surpassing the majority of current onboard clock schemes. Furthermore, it is advantageous in scenarios that require high real-time performance

in measurement, control, and navigation. Table 1 presents a comparison between the Allan deviation results obtained in the closed-loop experiment and those for existing GNSS onboard clocks, highlighting the significant advantages and potential of our proposal. The high-precision time and frequency reference on satellites can increase the accuracy and precision of various PNT applications. Additionally, such a synchronization-defined satellite virtual clock can be beneficial for space physics experiments, e.g., facilitating the provision of stable local heterodynes for the space very long baseline interferometry (SVLBI). SVLBI experiments typically require frequency stability below the 3×10^{-13} level within the integration time (10–100 s) of concern,[38,39] and our proposal may have the potential to fulfill this requirement (refer to Fig. 10).

Moreover, multiple ground stations simultaneously establishing their own satellite virtual clocks on the same GEO satellite would enable high-precision and real-time frequency comparison applications for distant Earth stations. On the premise of higher satellite clock recovery performance, the phase noise encountered by these recovered signals during the carrier down-link process is common-mode. Therefore, by simultaneously receiving these down-link carrier waves at any location within the satellite coverage area, real-time frequency variations between clocks of distant stations can be obtained. As the concept of the proposed satellite virtual clock is entirely based on the carrier phase, we believe that the frequency-transfer performance achieved using the aforementioned method can reach a level similar to that of TWCP,[34,35] which is also based on the Ku-band carrier phase of GEO satellites. This implies a cross-site frequency transfer accuracy at the level of picoseconds, which is orders of magnitude higher than those of the widely adopted TWSTFT and GPS CV/AV methods[40] (at the level of nanoseconds) in current UTC calculations.[41]

Because the proposed satellite virtual clock concept is considered entirely in the theory of special relativity, it does not take into account the phenomenon where light does not travel in a straight line in Earth's gravitational field with respect to the general relativity. We believe that the frequency/phase error in this case is negligible for ps-level time and frequency applications. However, the exact magnitudes of the resulting frequency/phase variations may need to be investigated further.

Table 1. Typical parameter comparison among the closed-loop results of this study and the measurement results of other GNSS constellations' onboard clocks.

Integrate time	Closed-loop results in this paper	GPS IIR Rb clocks[16]	BDS clocks[a][7,15]
10^2 s	10^{-14} ADEV level	10^{-12} ADEV level	10^{-13} ADEV level
10^3 s	10^{-15} ADEV level	10^{-13} ADEV level	10^{-14} ADEV level
10^4 s	10^{-16} ADEV level	10^{-14} ADEV level	10^{-14} ADEV level

[a]The best performance among BDS2-Rb, BDS3-Rb, and BDS3-PHM is selected.

7. Conclusion

This paper proposes the concept of a satellite virtual clock based on the carrier phase synchronization link between the ground and satellite. It also presents the principle and implementation of the beacon transponder used to realize this concept (corresponding payload is scheduled for launch in 2025). The innovation of this proposed satellite time and frequency reference lies in the following aspects. First, it does not require the additional incorporation of atomic clocks on the satellite, nor does it necessitate the introduction of additional complicated digital signal processing and servo systems. It only requires minor modifications to the existing commonly used GEO satellite transparent transponder structure for achieving the desired result. Second, the synchronization scheme for this type of onboard frequency reference is based on two-way information exchange between Earth and the satellite, with careful consideration given to the link asymmetry caused by the special relativistic effect (satellite Einstein synchronization). Third, the carrier phase is used as the medium for information exchange of the two-way link, theoretically enabling performance close to or even surpassing that of current onboard atomic clocks. For this type of synchronization-based onboard reference, the random phase noise and interference levels of the carrier synchronization link significantly influence the overall performance. Thus, a closed-loop experiment has been conducted using a commercial Ku-band GEO satellite to evaluate the random noise level of the carrier phase. The objective of this experiment is to quantify the difficult-to-model and difficult-to-eliminate random noise components in the ground–satellite link. Statistical analysis and the Shapiro–Wilk test have been performed on the measured phase noise results. The test results exhibit a remarkably close fit to a normal distribution, with a W statistic of 0.99974 and a p value of 0.82266. The obtained σ value for the one-week experiment in the 14.3135 GHz/12.5635 GHz Ku band is 0.633 ps, indicating the feasibility of achieving a σ value of 0.896 ps for a Ku-band four-way carrier link. In conclusion, we believe that ps-level synchronization/application performance can be achieved with the proposed system, which may have potential for a wide range of applications in the fields of physics, communication, and metrology.

Acknowledgements

This work was supported by the National Key Research and Development Program of China (Grant No. 2021YFA1402100). The authors are grateful to China Academy of Space Technology for the help in the preparation of this study.

References

[1] Barsocchi P, Celandroni N, Davoli F, Ferro E, Giambene G, Castano F J G, Gotta A, Moreno J I and Todorova P 2005 *Int. J. Satell. Commun. Network.* **23** 265
[2] Koudelka O and Schrotter P 2007 *Acta Astronaut.* **60** 986
[3] Minnett P J, Alvera-Azcarate A, Chin T M, Corlett G K, Gentemann C L, Karagali I, Li X, Marsouin A, Marullo S, Maturi E and others 2019 *Remote Sens. Environ.* **233** 111366
[4] Yang M, Xu F, Ren J G, Yin J, Li Y, Cao Y, Shen Q, Yong H L, Zhang L, Liao S K and others 2019 *Opt. Express* **27** 36114
[5] Zhan Y F, Wan P, Jiang C X, Pan X H, Chen X and Guo S 2020 *IEEE Wirel. Commun.* **27** 12
[6] Chawla I, Karthikeyan L and Mishra A K 2020 *J. Hydrol.* **585** 124826
[7] Wu Z Q, Zhou S S, Hu X G, Liu L, Shuai T, Xie Y H, Tang C P, Pan J Y, Zhu L F and Chang Z Q 2018 *GPS Solut.* **22** 1
[8] Huang G W, Cui B B, Xu Y and Zhang Q 2019 *Adv. Space Res.* **63** 2899
[9] Janis J P, Jones M R and Quackenbush N F 2021 *GPS Solut.* **25** 141
[10] Wang Q H, Droz F and Rochat P 2011 *Geomatics and Information Science of Wuhan University* **36** 1177
[11] Dong S W, Wu H T, Li X H, Guo S R and Yang Q W 2008 *Metrologia* **45** S47
[12] Burt E A, Prestage J D, Tjoelker R L, Enzer D G, Kuang D, Murphy D W, Robison D E, Seubert J M, Wang R T and Ely T A 2021 *Nature* **595** 43
[13] Qin W J, Ge Y L, Wei P, Dai P P and Yang X H 2020 *Measurement* **153** 107356
[14] Cao Y, Huang G W, Xie W, Xie S C and Wang H H 2021 *Acta Geodaetica et Geophysica* **56** 303
[15] Gu S F, Mao F Y, Gong X P, Lou Y D, Xu X Y and Zhou Y 2021 *Remote Sens-Basel.* **13** 5041
[16] Yao J, Yoon S, Stressler B, Hilla S and Schenewerk M 2021 *GPS Solut.* **25** 106
[17] Lee S W, Kim J, Jeong M S and Lee Y J 2011 *Adv. Space Res.* **47** 1654
[18] Zhou W, Ruan R G, Jia X L and Jin R 2020 *China Satellite Navigation Conference (CSNC) 2020 Proceedings* (Singapore: Springer) vol. 3 p. 134
[19] Cernigliaro A, Valloreia S, Galleani L and Tavella P 2013 *2013 International Conference on Localization and GNSS (ICL-GNSS)*, June 25–27, 2013, Turin, Italy, p. 1
[20] Tappero F, Dempster A, Iwata T, Imae M, Ikegami T, Fukuyama Y, Hagimoto K and Iwasaki A 2006 *Navigation* **53** 219
[21] Iwata T, Kawasaki Y, Imae M, Suzuyama T, Matsuzawa T, Fukushima S, Hashibe Y, Takasaki N, Kokubu K, Iwasaki A and others 2007 *Navigation* **54** 99
[22] Iwata T, Suzuyama T, Imae M, Hashibe Y and others 2010 *International Journal of Navigation and Observation* **2010** 604239
[23] Li X H, Wu H T, Bian Y J and Wang D N 2009 *Sci. China Ser. G* **52** 353
[24] Jing W F and Lu X C 2017 *2017 Joint Conference of the European Frequency and Time Forum and IEEE International Frequency Control Symposium (EFTF/IFCS)*, July 9–13, 2017, Besancon, France, p. 6
[25] Wu H T, Bian Y J, Lu X C, Li X H and Wang D N 2009 *Sci. China Ser. G* **52** 393
[26] Marlow B L S and Scherer D R 2021 *IEEE Trans. Ultrason. Ferr.* **68** 2007
[27] Diddams S A, Bergquist J C, Jefferts S R and Oates C W 2004 *Science* **306** 1318
[28] Nakamura T, Davila-Rodriguez J, Leopardi H, Sherman J A, Fortier T M, Xie X, Campbell J C, McGrew W F, Zhang X, Hassan Y S and others 2020 *Science* **368** 889
[29] Brewer S M, Chen J S, Hankin A M, Clements E R, Chou C W, Wineland D J, Hume D B and Leibrandt D R 2019 *Phys. Rev. Lett.* **123** 033201
[30] Zhang H, Ruan J, Liu D D, Yang F, Fan S C, Bai Y, Guan Y, Wang X L, Shi J R and Zhang S G 2022 *IEEE Trans. Instrum. Meas.* **71** 1
[31] Rovira-Garcia A, Juan J M, Sanz J, Gonzalez-Casado G, Ventura-Traveset J, Cacciapuoti L and Schoenemann E 2021 *Navigation-US* **68** 815
[32] Fonville B, Matsakis D, Pawlitzki A and Schaefer W 2004 *Proceedings of the 36th Annual Precise Time and Time Interval Systems and Applications Meeting*, 7–9 December, 2004, Washington DC, p. 149
[33] Fujieda M, Gotoh T and Amagai J 2016 *J. Phys.: Conf. Ser.* **723** 012036
[34] Fujieda M, Piester D, Gotoh T, Becker J, Aida M and Bauch A 2014 *Metrologia* **51** 253
[35] Fujieda M, Gotoh T, Nakagawa F, Tabuchi R, Aida M and Amagai J 2012 *IEEE Trans. Ultrason. Ferr.* **59** 2625
[36] Nakagawa F, Amagai J, Tabuchi R, Takahashi Y, Nakamura M, Tsuchiya S and Hama S 2013 *Metrologia* **50** 200
[37] Shapiro S S and Wilk M B 1965 *Biometrika* **52** 591
[38] Gurvits L I 2020 *Adv. Space Res.* **65** 868
[39] D'Addario L R 1991 *IEEE T. Instrum. Meas.* **40** 584
[40] Piester D and Schnatz H 2009 *PTB-Mitteilungen* **119** 33
[41] Panfilo G and Arias F 2019 *Metrologia* **56** 042001